Supporting Information

Lee et al. 10.1073/pnas.1215175109

SI Text

SI Materials and Methods. ***Cloning of photoactivatable fluorescent protein (PA-FP) gene.*** To generate PA-FPs fused to avitag at the C terminus and His-tag at the N terminus of the proteins, we first constructed pJY00 by cloning His (His-tag) upstream of the avitag gene in pAC4 (Avidity). Then, mEos2 or Dendra2 genes were obtained by PCR from prSETA and pDendra2, respectively. mEos2 or Dendra2 were cloned into the XmaI site of pJY00 to generate pJY01 or pJY02, respectively. All these three genes (avitag, mEos2 or Dendra2, His-tag) were in frame, and under the control of the Trc promoter, which is inducible by IPTG.

Expression and in vivo biotinylation of PA-FPs. mEos2 or Dendra2 were overexpressed and biotinylated in vivo following the induction procedure for avi-tagged proteins (Avidity) with few modifications. AVB101 (an *Escherichia coli* B strain that contains pBirACm, an IPTG inducible plasmid containing the BirA gene; Avidity) transformed with the plasmids pJY01 or pJY02 was inoculated on an LB plate supplemented with 10 μg/mL of chloramphenicol (cam) and 100 μg/mL of ampiciline (amp). A single colony was transferred into LB media supplemented with cam and amp, and incubated overnight at 37 °C. A 0.5 mL of this cell culture was transferred into 150 mL of LB-amp and shaken at 37 °C. When OD_{600} reached 0.7, biotin (50 μM final concentration) and IPTG (200 μM final concentration) solution were added to the cell culture and the expression of the protein was induced for 3 h. The cells were concentrated by centrifugation, washed two times with lysis buffer (50 mM sodium phosphate pH 7.4, 300 mM NaCl, 10 mM Imidazol, 5% glycerol) and then purified or stored at −80 °C.

Purification of PA-FP. mEos2 and Dendra2 were purified by affinity chromatography using nickel sepharose (His-trap HP; GE) by following a standard His-tagged protein purification protocol. A cell pellet from 150 mL cell culture was suspended in 10 mL of lysis buffer and sonicated (five pulses of 20 s, 18 mW with 1 min interval). The soluble fraction was separated from the insoluble one by centrifugation at 4 °C, 48,400 × g for 1 h. The supernatant was loaded onto the nickel column at a flow rate of 0.5 mL/min and washed with lysis buffer at 1 mL/min. Bound proteins were eluted by loading elution buffer (50 mM sodium phosphate pH 7.4, 300 mM NaCl, 150 mM Imidazol, 5% glycerol) at 1 mL/min onto the column and fractions containing only mEos2 or Dendra2 were combined, concentrated, and dialyzed against 50 mM sodium phosphate pH 7.4, 300 mM NaCl, 5% glycerol. The concentration of the protein was calculated by using the extinction coefficient at 488 nm. As observed in Fig. S1, the purified Dendra2 proteins were pure (SDS-PAGE), fluorescent (in-gel fluorescence), and biotinylated (Western blot analysis using streptavidin conjugated with horseradish peroxidase). The same results were observed for mEos2 purification. The purified proteins were fast frozen and kept at −80 °C.

Coverslip cleaning and streptavidin coating. Glass coverslips were cleaned by sonication in acetone and ethanol for 30 and 15 min, respectively. After rinsing with Milli-Q filtered water, the coverslips were boiled in 1 M potassium hydroxide for 30 min, cooled down, and rinsed again with water. Subsequently, the coverslips were immersed in a 4:9 solution of hydrogen peroxide and sulfuric acid for 60 min and rinsed again with water, then with acetone, and stored in water until use.

Cleaned coverslips were dried with filtered N_2 gas and incubated in a 1% silane [(3-aminopropyl)triethoxysilane; Sigma-Aldrich 440140] solution in acetone for 30 min. The solution was discarded, fresh acetone added, and the coverslips sonicated for 5 min. This step was repeated two more times and followed by two more sonications, but carried out in methanol instead of acetone. Silane-coated coverslips were rinsed with Milli-Q water thoroughly and dried with N_2 gas. Fifty microliters of 20% biotin-PEG:PEG (1:9 wt/wt ratio; Biotin-PEG-SC-5000 and mPEG-SCM-5000; Laysan Bio, Inc.) solution (dissolved in 0.1 M $NaHCO_3$ pH 8.0) was spotted between two coverslips and incubated overnight (at least 6 h) in a humid environment. Nonbound PEG was removed from the coverslips by rinsing with water, and the coverslips were finally stored in Milli-Q water until use (good for up to 2 months).

Protein immobilization. To immobilize mEos2 or Dendra2, first, the biotin-coated glass coverslip was incubated with streptavidin (10 μg/mL in Tris buffer, 150 mM Tris pH 7.4, 50 mM NaCl) for 10 min, then with fiducial biotin-gold nanoparticles (100 nm diameter; Nanopartz Inc., 20-PB-100-50) for 5 min and washed with Tris buffer in between. Finally, 50 μL of 0.2 nM protein solution was deposited and incubated on the coverslip for 10 min and washed with Tris buffer. Around 200 molecules were dispersed in a 35 μm × 35 μm field of view (Fig. S3 *A*–*C*).

Instrumentation. The photoactivated localization microscopy (PALM) instrument was built on a commercial Olympus IX71 fluorescence microscope with two lasers, wavelengths 561 nm (Sapphire 561 nm, 200 mW; Coherent, Inc.) and 405 nm (Cube, 405 nm, 50 mW; Coherent, Inc.), and an Olympus UAPO150xO/TIRFM-SP N.A. 1.45 objective. The two lasers were combined, magnified, and focused on the back focal plane of the objective to illuminate a sample area of 55 μm × 55 μm. The power of the 561 nm laser was fixed to 22 W/mm^2 throughout all the experiments. Fluorescence images were acquired by a low-noise, light-sensitive electron multiplying charge coupled device (DV887ECS-BV; Andor) at 20 Hz with an emission filter for mEos2 and Dendra2. Focus drift was stabilized by active feedback control of a piezo-stage (CRIFF, ASI) whereas in-plane sample drift was corrected by the localization of Au fiducials with nanometer accuracy (1).

Data acquisition for the in vitro experiments. Characterization of blinking kinetics: The sample was illuminated for 2 min with the 405 nm activation laser at 9.1 mW/mm^2; then it was turned off and the 561 nm excitation laser at 22 mW/mm^2 was turned on for acquiring 3,000 frames. Characterization of the photoactivation rate at different laser powers: The sample was illuminated with the activation laser at a constant power (0, 1.5, 3.4, 5.3, 7.2, or 9.1 mW/mm^2), simultaneously with the excitation laser. Fermi activation scheme: The sample was illuminated with the excitation laser simultaneously with the activation laser, whose power varied in time according to the Fermi activation scheme (Eq. **S40**).

Cell strain, cell preparation, and PALM data acquisition for FliM-dendra2 counting. Δ*fliM* strain (DFB190 from Prof. Howard Berg at Harvard University, Cambridge, MA) (2) was transformed with pJY03 (plasmid containing *fliM* fused to *dendra2* at the carboxyl-terminal, linker between FliM and Dendra2 is ArgSer). pJY03 is

a plasmid constructed from pFS6003m, a derivative of pBAD (3), where the gene for EGFP was replaced by *dendra2*. Therefore the expression of FliM-Dendra2 is inducible by arabinose.

Overnight cell culture was diluted 1:100 in tryptone broth (TB; 1% tryptone and 0.5% NaCl) and grown at 34 °C for about 4 h, to an OD_{600} of 0.4–0.5, in presence of 0.001% of arabinose. Cells were concentrated by centrifugation, washed, and resuspended in tethering buffer (TEB; 10 mM potassium phosphate, 0.1 mM EDTA, 1 mM L-methionine, 67 mM sodium chloride, 10 mM sodium lactate, pH 7). Flagella were sheared by passing the cell suspension back and forth 50 times between two syringes with 26 $\frac{1}{2}$-gauge needles connected by approximately 20 cm of thin polyethylene tubing. After shearing, cell suspension was washed and concentrated in TEB, deposited on the cleaned poly-L-lysine-coated coverslip and sandwiched with a cleaned coverslip.

PALM data for FliM-Dendra2 was acquired by continuous illumination of 561 nm laser with power fixed at 22 W/mm^2 and 405 nm laser modulated to follow Fermi activation (Eqs. **4** and **5**; Fig. 4 *D* and *E*). The Fermi activation parameters were $t_F = 2.2$ min and $T = 12$ s. To assure that all the Dendra2 molecules were activated, the 405 nm laser was set to the maximum available power at time 3 min of data acquisition and followed until 3.3 min.

PALM data analysis. Individual emission bursts were detected and localized by a custom-developed PALM analysis software written in Matlab, and based on well-established algorithms (4, 5). An EMCCD output was first converted to photon counts to obtain calibrated images (6), which were searched for local peaks above a certain threshold (approximately 8 times brighter than the background noise). A two-dimensional Gaussian point spread function was fitted to a 9×9 pixel block cropped around each local peak, to obtain the position of the molecule with subdiffraction accuracy. If a local peak was found to persist across multiple consecutive frames, the blocks cropped in each of these frames were attributed to a single identical molecule, and were therefore summed before the fitting. Finally, the emission bursts were grouped into individual molecules according to their pairwise spatial separation, using the Hoshen–Kopelman clustering algorithm (7).

Simulations of counting and identification algorithms. Emission traces for individual proteins were generated by drawing the transition times at random, from an exponential (constant 405 nm laser power) or uniform (Fermi activation scheme) distribution for the activation, from an exponential distribution for the transition to the dark state and photobleaching, and from a biexponential distribution for the recovery from the dark state. Then, they were superimposed to simulate a trace that would be obtained from multiple spatially indistinguishable molecules.

To find the optimal τ_c for a given number of molecules N_{mol}, we generated 1,500 traces with that number of molecules. For each trace, while pretending to ignore the molecular identity of the bursts, we counted $N_b^{(\tau_c)}$ using each value of τ_c between 0 and 1.5 s for Dendra2 and 0 and 10 s for mEos2, by steps of 1 ms. Finally, we chose the value of τ_c for which the average count $\langle N_b^{(\tau_c)} \rangle$ was the closest to N_{mol}. This value gave us a calibration curve like the one presented in Fig. 5*B*.

Then, we generated 1,500 other traces, that again contained the same number of molecules. These traces were counted using the iterative optimal-τ_c method (Fig. 5*C*): Starting from $\tau_c = 0$, we counted $N_b^{(\tau_c)}$, updated τ_c by referencing to the already obtained calibration curve, and repeated the procedure until convergence.

On the same traces, we also tested counting by the average-blinking normalization method: We divided the number of temporally resolved bursts by the theoretical mean number of bursts per molecule, $1 + \langle N_{\mathrm{blink}} \rangle$.

Finally, we compared the burst groupings yielded by iterative optimal-τ_c counting to the actual molecular identities. Only a group that contained all the signals from a single molecule was considered to identify a molecule correctly.

We were thus able to compute the mean and standard deviation of the iterative optimal-τ_c counting method and the average-blinking normalization method, as well as the misidentification rate of the iterative optimal-τ_c counting method. We repeated that process for numbers of molecules N_{mol} ranging from 1 to 400 and experiment durations ranging from 1 min to 1 h in 1 min steps. The results are presented in Fig. 6 and in Figs. S7 and S8.

In addition, we wished to know how robust was the iterative optimal-τ_c counting method to the changes in the blinking kinetic rates used in the analysis. To this end, we carried out simulation studies by varying the kinetic rates around the values determined in vitro. We first computed the optimal-τ_c curve using the rates measured in vitro. Then, we varied one of the kinetic rates (k_{d}, k_r, or k_{b}) while the other two were kept at their in vitro values, and generated sets of traces using these new rates [as recovery from the dark state is nearly monoexponential for Dendra2 (Fig. 2 and Fig. S4), we assumed for simplicity a monoexponential recovery with rate k_r] and our in vivo experimental parameters of $N_{\mathrm{mol}} = 34$ and $t_F = 2.2$ min. We then counted molecules from these sets of traces using the previously computed optimal-τ_c curve. The mismatch between the rates led to a bias error, whose amplitude quantifies how robust the optimal-τ_c counting is against such mismatches. We tabulated this error and plotted it in Fig. S9.

SI Discussion. ***Poissonian recovery from a dark state.*** The dwell time probability distribution of a Poisson process (i.e., the probability that an event occurs between t and $t + dt$) is given by

$$p_k(t) = ke^{-kt}, \qquad \textbf{[S1]}$$

and the probability that no event happens between times 0 and t in the Poisson process is given by

$$q_k(t) \equiv 1 - \int_0^t dt p_k(t) = e^{-kt}. \qquad \textbf{[S2]}$$

In the proposed kinetic model of fluorescence blinking as shown in Fig. S2*A*, the probability that a fluorescent molecule is photobleached at time t with no blink is

$$P(0,t) = p_{k_b}(t) q_{k_d}(t). \qquad \textbf{[S3]}$$

Similarly, the probability that exactly one blink happened before photobleaching at time t (Fig. S2) is

$$\begin{aligned} P(1,t) &= \int_0^t dt_1 \{p_{k_d}(t_1) q_{k_b}(t_1)\} \\ &\quad \times \left(\int_0^{t-t_1} d\tau p_{k_r}(\tau) \{p_{k_b}(t - t_1 - \tau) q_{k_d}(t - t_1 - \tau)\} \right) \\ &= \int_0^t dt_1 w_1(t_1) \left(\int_0^{t-t_1} d\tau p_{k_r}(\tau) w_2(t - t_1 - \tau) \right) \end{aligned} \qquad \textbf{[S4]}$$

where

$$w_1(t) = p_{k_{\mathrm{d}}}(t) q_{k_{\mathrm{b}}}(t), \qquad w_2(t) = p_{k_{\mathrm{b}}}(t) q_{k_{\mathrm{d}}}(t). \qquad \textbf{[S5]}$$

We can rewrite Eq. **S4** by using the convolution operator,

$$P(1,t) = (w_1 \otimes p_{k_r} \otimes w_2)(t), \qquad \textbf{[S6]}$$

where the convolution of two arbitrary functions $f(t)$ and $g(t)$ is defined by

$$(f \otimes g)(t) \equiv \int_0^t dt' f(t') g(t-t'). \quad \textbf{[S7]}$$

Thus, the joint probability distribution of photobleaching time t and number of blinks n can be written in a simple form, as follows:

$$P(n,t) = \underbrace{(w_1 \otimes p_{k_r}) \otimes \cdots \otimes (w_1 \otimes p_{k_r})_n}_{n} \otimes w_2. \quad \textbf{[S8]}$$

The multiple convolutions in Eq. **S8** complicates the calculation in time. To simplify and speed up the calculation, we use the Laplace transform and the convolution theorem. Accordingly,

$$\tilde{P}(n,s) \equiv \mathscr{L}\{P(n,t)\} \equiv \int_0^\infty P(n,t) e^{-st} dt = (\tilde{w}_1(s)\tilde{p}_{k_r}(s))^n \tilde{w}_2(s), \quad \textbf{[S9]}$$

where $\tilde{w}_1(s)$, $\tilde{p}_{k_r}(s)$, and $\tilde{w}_2(s)$ are the Laplace transforms of $w_1(t)$, $p_{k_r}(t)$, and $w_2(t)$, respectively, and are easily calculated to be

$$\tilde{w}_1(s) = \frac{k_d}{s + k_d + k_b},$$
$$\tilde{p}_{k_r}(s) = \frac{k_r}{s + k_r}, \quad \text{and}$$
$$\tilde{w}_2(s) = \frac{k_b}{s + k_d + k_b}. \quad \textbf{[S10]}$$

Therefore,

$$\tilde{P}(n,s) = \left(\frac{k_d}{s + k_d + k_b}\frac{k_r}{s + k_r}\right)^n \frac{k_b}{s + k_d + k_b}. \quad \textbf{[S11]}$$

Although the probability distribution in time can in principle be calculated by inverse Laplace transform of Eq. **S11**, its momenta can be easily calculated even without calculating the inverse transform, as follows.

Mean number of blinks:

$$\langle N_{\text{blink}} \rangle = \sum_{n=0}^\infty n \int_0^\infty P(n,t) dt = \sum_{n=0}^\infty n \tilde{P}(n, s=0) = \frac{k_d}{k_b}. \quad \textbf{[S12]}$$

Mean photobleach time:

$$\langle T_{\text{bleach}} \rangle = \sum_{n=0}^\infty \int_0^\infty t P(n,t) dt$$
$$= -\sum_{n=0}^\infty \frac{\partial \tilde{P}(n,s)}{\partial s}\bigg|_{s=0} = \frac{1}{k_b}\left(1 + \frac{k_d}{k_r}\right). \quad \textbf{[S13]}$$

Similarly, the probability distribution of the number of blinks and the probability density function (PDF) of the photobleach time can be calculated, as follows.

Probability distribution of the number of blinks:

$$P(N_{\text{blink}} = n) = \int_0^\infty P(n,t) dt = \tilde{P}(n, s=0) = \eta^n (1-\eta) \quad \textbf{[S14]}$$

where

$$\eta \equiv \frac{k_d}{k_d + k_b} \quad \textbf{[S15]}$$

is the probability of going to the dark state, rather than to the photobleach state. Noticeably, Eq. **S14** is a geometric distribution, which gives the probability of n consecutive successes, in a sequence of Bernoulli trials with success probability η, before the first failure occurs.

PDF of photobleach time:

$$\frac{P(t \le T_{\text{bleach}} \le t + dt)}{dt} = \mathscr{L}^{-1}\left\{\sum_{n=0}^\infty \tilde{P}(n,s)\right\}$$
$$= \mathscr{L}^{-1}\left\{\frac{k_b(s + k_r)}{s^2 + (k_d + k_b + k_r)s + k_b k_r}\right\}$$
$$= \mathscr{L}^{-1}\left\{\frac{k_b(s + k_r)}{(s + k_1)(s + k_2)}\right\}$$
$$= \frac{1}{1 + \alpha_r}\left\{k_1 e^{-k_1 t} + \alpha_r k_2 e^{-k_2 t}\right\} \quad \textbf{[S16]}$$

where

$$k_1 \equiv \frac{1}{2}\{(k_d + k_b + k_r) - \sqrt{(k_d + k_b + k_r)^2 - 4k_b k_r}\}, \quad \textbf{[S17]}$$

$$k_2 \equiv \frac{1}{2}\{(k_d + k_b + k_r) + \sqrt{(k_d + k_b + k_r)^2 - 4k_b k_r}\}, \quad \textbf{[S18]}$$

$$\alpha_r \equiv \frac{k_1(k_2 - k_r)}{k_2(k_r - k_1)}. \quad \textbf{[S19]}$$

Non-poissonian recovery from two dark states. Experimentally, the dark state dwell time distribution of mEos2 is well-described by a double exponential function. This observation implies the existence of two dark states, as in Fig. S2*C*. The Laplace transform of the joint probability distribution of the photobleach time t and the number of blinks n is formally the same as Eq. **S9** with $\tilde{p}_{k_r}(s)$ replaced by a more general non-Poissonian dwell time distribution function $\tilde{p}_r(s)$:

$$\tilde{P}(n,s) = (\tilde{w}_1(s)\tilde{p}_r(s))^n \tilde{w}_2(s). \quad \textbf{[S20]}$$

For a double exponential dwell time distribution, $\tilde{p}_r(s)$ is given by

$$\tilde{p}_r(s) = \frac{1}{1 + \alpha}\left(\frac{k_{r1}}{s + k_{r1}} + \alpha\frac{k_{r2}}{s + k_{r2}}\right) = \frac{\bar{k}_r s + k_{r1}k_{r2}}{(s + k_{r1})(s + k_{r2})}, \quad \textbf{[S21]}$$

where $\bar{k}_r \equiv (k_{r1} + \alpha k_{r2})/(1 + \alpha)$ is the average recovery rate. Accordingly,

$$\tilde{P}(n,s) = \left(\frac{k_d}{s + k_d + k_b}\frac{\bar{k}_r s + k_{r1}k_{r2}}{(s + k_{r1})(s + k_{r2})}\right)^n \frac{k_b}{s + k_d + k_b}. \quad \textbf{[S22]}$$

The probability distribution of number of blinks, independently of the kinetics of recovery from the dark states, is still given by Eq. **S14**. On the other hand, the mean value and the PDF of the photobleach time are changed, as follows.

Mean photobleach time:

$$\langle T_{\text{bleach}} \rangle = -\sum_{n=0}^\infty \frac{\partial \tilde{P}(n,s)}{\partial s}\bigg|_{s=0} = \frac{1}{k_b}(1 + k_d \bar{\tau}_r), \quad \textbf{[S23]}$$

where $\bar{\tau}_r \equiv (1/k_{r1} + \alpha/k_{r2})/(1 + \alpha)$ is the average dwell time in dark states.

PDF of photobleach time:

$$\frac{P(t \le T_{\text{bleach}} \le t+dt)}{dt} = \mathscr{L}^{-1}\left\{\sum_{n=0}^{\infty}\tilde{P}(n,s)\right\}$$
$$= \mathscr{L}^{-1}\left\{\frac{k_b(s+k_{r1})(s+k_{kr2})}{s^3+as^2+bs+c}\right\}$$
$$= \mathscr{L}^{-1}\left\{\frac{k_b(s+k_{r1})(s+k_{r2})}{(s+k_1)(s+k_2)(s+k_3)}\right\}$$
$$= k_b\{r_1e^{-k_1t}+r_2e^{-k_2t}+r_3e^{-k_3t}\}, \quad \textbf{[S24]}$$

where

$$a = k_d + k_b + k_{r1} + k_{r2},$$
$$b = (k_{r1}+k_{r2}-\bar{k}_r)k_d + (k_{r1}+k_{r2})k_b + k_{r1}k_{r2},$$
$$c = k_bk_{r1}k_{r2}, \quad \textbf{[S25]}$$

k_1, k_2, and k_3 are solutions of a cubic equation, obtained by factorizing the denominator of Eq. **S24**, and

$$r_1 = \frac{(k_{r1}-k_1)(k_{r2}-k_1)}{(k_2-k_1)(k_3-k_1)},$$
$$r_2 = \frac{(k_{r1}-k_2)(k_{r2}-k_2)}{(k_1-k_2)(k_3-k_2)}, \quad \text{and}$$
$$r_3 = \frac{(k_{r1}-k_3)(k_{r2}-k_3)}{(k_1-k_3)(k_2-k_3)}. \quad \textbf{[S26]}$$

Cutoff effect of dark state dwell time in blinking number probability. Because of the blinking of PA-FPs, it is important to introduce a cutoff for the dwell time in the dark state so that the blinking can be attributed to the fluorescence of the same molecule and therefore improve the identification of single molecules. Previous PALM reconstruction algorithms used a fixed cutoff value between 1.5 and 15 s (4, 8, 9). However, the choice of these values was purely empirical.

Here, we calculate the probability distribution of the number of blinks whose dwell time in the dark state is longer than an arbitrarily given cutoff value. For that, we first introduce a joint probability distribution function,

$P(m,t;n,\tau_c)$: The probability that the number of blinks with dark state dwells longer than τ_c is m, given that photobleaching occurs between times t and $t+dt$ and that the total number of blinks is n ($m \le n$).

Following a mathematical induction similar to the derivation of Eqs. **S3–S9** , we can calculate the probability distribution function.

For 0 total blink ($n=0$):

$$P(m=0,t;n=0,\tau_c) = p_{k_b}(t)q_{k_d}(t).$$

For 1 total blink ($n=1$):

$m=0$:

$$P(m=0,t;n=1,\tau_c)$$
$$= \int_0^t dt_1 w_1(t_1)\left(\int_0^{t-t_1} d\tau[p_r(\tau)L(\tau-\tau_c)]w_2(t-t_1-\tau)\right)$$
$$= (w_1 \otimes p_r^{(L)} \otimes w_2)(t) \quad \textbf{[S27]}$$

$m=1$:

$$P(m=1,t;n=1,\tau_c)$$
$$= \int_0^t dt_1 w_1(t_1)\left(\int_0^{t-t_1} d\tau[p_r(\tau)H(\tau-\tau_c)]w_2(t-t_1-\tau)\right)$$
$$= (w_1 \otimes p_r^{(H)} \otimes w_2)(t), \quad \textbf{[S28]}$$

where $H(t)$ is the Heaviside step function and $L(t) \equiv 1-H(t)$, as shown in Fig. S2 *D* and *E*,

$$p_r^{(H)}(t) = p_r(t)H(t-\tau_c), \quad \text{and} \quad p_r^{(L)}(t) = p_r(t)L(t-\tau_c). \quad \textbf{[S29]}$$

In general, we can write

$$P(m,t;n,\tau_c) = \binom{n}{m}\underbrace{(w_1 \otimes p_r^{(H)}) \otimes \cdots \otimes (w_1 \otimes p_r^{(H)})}_{m}$$
$$\otimes \underbrace{(w_1 \otimes p_r^{(L)}) \otimes \cdots \otimes (w_1 \otimes p_r^{(L)})}_{n-m} \otimes w_2, \quad \textbf{[S30]}$$

whose Laplace transform is given by

$$\tilde{P}(m,s;n,\tau_c) = \binom{n}{m}\tilde{w}_1^n(s)(\tilde{p}_r^{(H)}(s))^m(\tilde{p}_r^{(L)}(s))^{n-m}\tilde{w}_2(s). \quad \textbf{[S31]}$$

Practically, we are interested in the number of blinks with the dark state dwell longer than τ_c, irrespective of the exact total number of blinks. This PDF, denoted by $P(m,t;\tau_c)$, can be obtained by summing over n in Eq. **S31**.

$$\tilde{P}(m,s;\tau_c) = \sum_{n=m}^{\infty}\tilde{P}(m,s;n,\tau_c)$$
$$= \sum_{n=m}^{\infty}\binom{n}{m}\tilde{w}_1^n(\tilde{p}_r^{(H)})^m(\tilde{p}_r^{(L)})^{n-m}\tilde{w}_2$$
$$= \sum_{l=0}^{\infty}\binom{l+m}{m}(\tilde{w}_1\tilde{p}_r^{(L)})^l(\tilde{w}_1\tilde{p}_r^{(H)})^m\tilde{w}_2$$
$$= \frac{(\tilde{w}_1\tilde{p}_r^{(H)})^m\tilde{w}_2}{(1-\tilde{w}_1\tilde{p}_r^{(L)})^{m+1}}. \quad \textbf{[S32]}$$

The Laplace transforms $\tilde{p}_r^{(H)}(s)$ and $\tilde{p}_r^{(L)}(s)$ of a double exponential dwell time distribution function $p_r(t)$ are given by

$$\tilde{p}_r^{(H)}(s) = \frac{1}{1+\alpha}\left(\frac{k_{r1}}{s+k_{r1}}\gamma_1(s) + \alpha\frac{k_{r2}}{s+k_{r2}}\gamma_2(s)\right)$$

$$\tilde{p}_r^{(L)}(s) = \frac{1}{1+\alpha}\left(\frac{k_{r1}}{s+k_{r1}}(1-\gamma_1(s)) + \alpha\frac{k_{r2}}{s+k_{r2}}(1-\gamma_2(s))\right) \quad \textbf{[S33]}$$

where

$$\gamma_1(s) = e^{-(s+k_{r1})\tau_c}, \quad \text{and} \quad \gamma_2(s) = e^{-(s+k_{r2})\tau_c}. \quad \textbf{[S34]}$$

By using these results and Eq. **S10**, we can finally calculate the probability distribution of the number of blinks with dark state dwell time longer than a cutoff value τ_c regardless of the photobleach time:

$$P(N_{\text{blink}} = n; \tau_c) = \int_0^\infty P(n, t; \tau_c)dt = \tilde{P}(n, s = 0; \tau_c)$$
$$= \bar{\eta}^n(1 - \bar{\eta}), \qquad \text{[S35]}$$

where

$$\bar{\eta} \equiv \frac{p_{\tau_c}\eta}{1 - \eta + p_{\tau_c}\eta},$$
$$\eta = \frac{k_d}{k_d + k_b}, \quad \text{and}$$
$$p_{\tau_c} = \frac{e^{-k_{r1}\tau_c} + \alpha e^{-k_{r2}\tau_c}}{1 + \alpha}. \qquad \text{[S36]}$$

Remarkably, Eq. **S35** still has the form of a geometric distribution. However, when it is compared to Eq. **S14**, the probability to go to the dark state, η, is replaced by an effective dark state transition probability, $p_{\tau_c}\eta$, which is reduced by the factor p_{τ_c} that exponentially decays in the cutoff value τ_c. Therefore, the overcounting error by blinking could be reduced dramatically by using reasonable values of τ_c, that effectively decrease the apparent dark state transition probability.

Fermi activation. The dwell time probability distribution $p_k(t)$ of an inhomogeneous Poisson process in which the rate $k(t)$ varies in time satisfies

$$p_k(t) = k(t)\left(1 - \int_0^t p_k(t')dt'\right); \qquad \text{[S37]}$$

i.e., the probability that an event happens between times t and $t + dt$ is given by product of the rate at the time t and the probability that no event has happened until then. Solving for $p_k(t)$ gives

$$p_k(t) = k(t)e^{-\int_0^t k(t')dt'}. \qquad \text{[S38]}$$

By definition, the dwell time probability distribution $p_F(t)$ for a Fermi activation scheme is given by a Fermi function,

$$p_F(t) = \frac{A}{1 + e^{(t-t_F)/T}}, \qquad A = \frac{1}{T\ln(1 + e^{t_F/T})}, \qquad \text{[S39]}$$

where t_F is the time at which the Fermi function drops to half the maximum, and T is the fall-off time of the Fermi function. From Eqs. **S38** and **S39**, we get the time-varying activation rate $k_a(t)$ required for the Fermi activation scheme,

$$k_a(t) = \frac{1}{T}\frac{e^{-(t-t_F)/T}}{(1 + e^{-(t-t_F)/T})\ln(1 + e^{-(t-t_F)/T})}. \qquad \text{[S40]}$$

Distribution of N_{c1} and counting by blinking correction. Although the probability distributions of N_b and N_{c2} are too complicated to be expressed analytically, the probability distribution of N_{c1} (the sum of the number of molecules N_{mol} and the total number of blinks) is given by a negative binomial distribution, which is the generalization of the geometric distribution Eq. **S35** to multiple molecules,

$$P(N_{c1} - N_{\text{mol}} = n) = \binom{n + N_{\text{mol}} - 1}{m}\bar{\eta}^n(1 - \bar{\eta})^{N_{\text{mol}}},$$
$$n = 0, 1, 2, \ldots \qquad \text{[S41]}$$

In particular, this distribution has a mean of

$$\langle N_{c1}\rangle = \frac{N_{\text{mol}}}{1 - \bar{\eta}} = N_{\text{mol}}(1 + \langle N_{\text{blink}}\rangle) \qquad \text{[S42]}$$

and a standard deviation of

$$\sigma_{N_{c1}} = \sqrt{N_{\text{mol}}}\frac{\sqrt{\bar{\eta}}}{1 - \bar{\eta}}. \qquad \text{[S43]}$$

When $\tau_c = 0$ and thus $\bar{\eta} = \eta$, N_{c1} is just the total number of bursts (assuming that there is no overlap between the bursts; i.e., that the bursts are temporally resolved).

As a consequence,

$$\frac{N_{c1}(\tau_c = 0)}{1 + \langle N_{\text{blink}}\rangle} \qquad \text{[S44]}$$

is an unbiased estimator of the number of molecules, with standard deviation

$$\sigma = \frac{\sigma_{N_{c1}}}{1 + \langle N_{\text{blink}}\rangle} = \sqrt{N_{\text{mol}}\eta}. \qquad \text{[S45]}$$

1. Yildiz A, et al. (2003) Myosin V walks hand-over-hand: Single fluorophore imaging with 1.5-nm localization. *Science* 300:2061–2065.
2. Sourjik V, Berg H (2000) Localization of components of the chemotaxis machinery of *Escherichia coli* using fluorescent protein fusions. *Mol Microbiol* 37:740–751.
3. Fukuoka H, Inoue Y, Terasawa S, Takahashi H, Ishijima A (2010) Exchange of rotor components in functioning bacterial flagellar motor. *Biochem Biophys Res Commun* 394:130–135.
4. Betzig E, et al. (2006) Imaging intracellular fluorescent proteins at nanometer resolution. *Science* 313:1642–1645.
5. Fleming TC, et al. (2010) Dynamic SpoIIIE assembly mediates septal membrane fission during *Bacillus subtilis* sporulation. *Genes Dev* 24:1160–1172.
6. Ulbrich MH, Isacoff EY (2007) Subunit counting in membrane-bound proteins. *Nat Methods* 4:319–321.
7. Al-Futaisi A, Patzek T (2003) Extension of Hoshen-Kopelman algorithm to non-lattice environments. *Physica A* 321:665–678.
8. Subach FV, et al. (2009) Photoactivatable mCherry for high-resolution two-color fluorescence microscopy. *Nat Methods* 6:153–159.
9. Annibale P, Vanni S, Scarselli M, Rothlisberger U, Radenovic A (2011) Identification of clustering artifacts in photoactivated localization microscopy. *Nat Methods* 8:527–528.

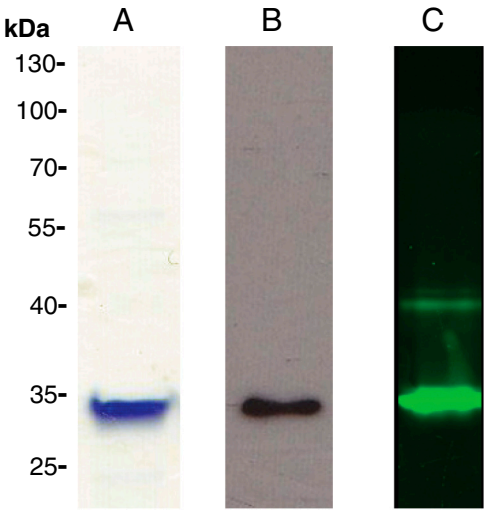

Fig. S1. Purified Dendra2 protein (as described in *SI Materials and Methods*) shows a single band at the expected molecular weight by (*A*) Coomassie blue stained SDS-PAGE. This protein is (*B*) biotinylated and (*C*) fluorescent in a semidenaturant SDS-PAGE. (*Left*) Molecular weight is labeled.

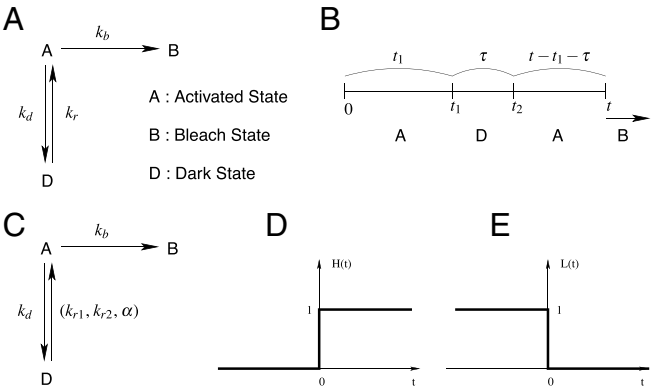

Fig. S2. (*A*) A simple kinetic model of mEos2 blinking. (*B*) Definition of transition time points in the case of a molecule that photobleaches after one blink. (*C*) Modified model for two dark states. The dwell time distribution is given by a double exponential function with two decay constants k_{r1} and k_{r2}. Here, α is the ratio between the number of recovery events from a dark state with rates k_{r2} and k_{r1}. (*D*) Heaviside step function $H(t)$. (*E*) Left-sided step function $L(t) = 1 - H(t)$.

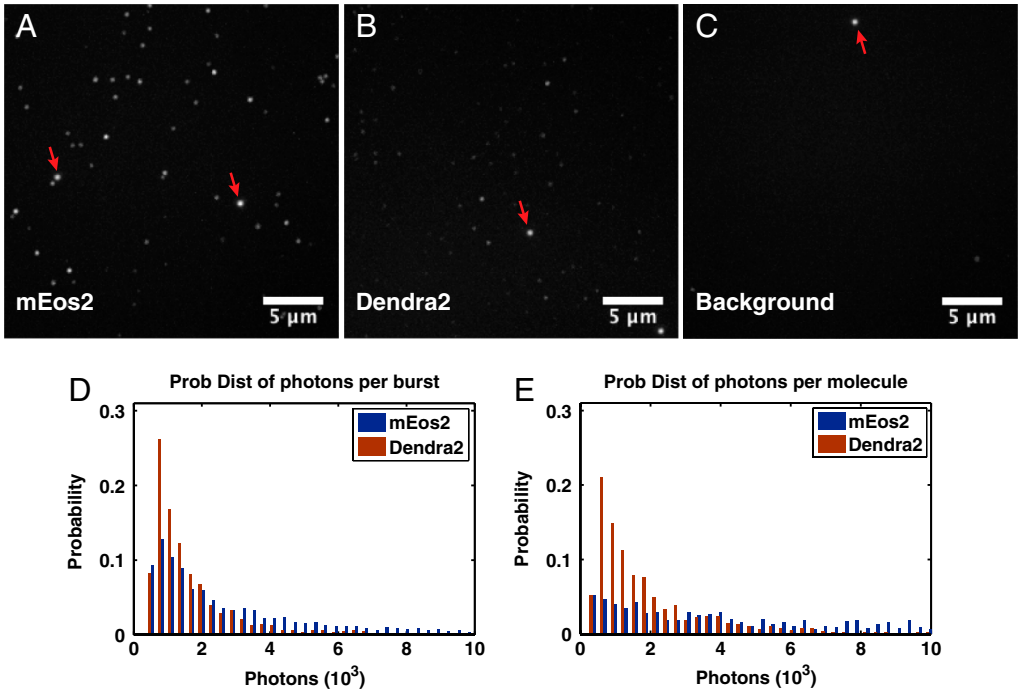

Fig. S3. Individual mEos2 (*A*) and Dendra2 (*B*) proteins are separated by at least 300 nm from each other in this field of view, as shown in a diffraction-limited image (*A*, *B*, and *C* show a 28 μm × 28 μm area cropped from the entire 35 μm × 35 μm field of view and employed for the single molecule analysis). In each field of view, a total of approximately 200 molecules and approximately four gold nanospheres (red arrows) were immobilized on the glass coverslip in Tris buffer. We analyzed at least four different fields (total number of molecules was approximately 800) for both proteins. (*C*) A control experiment that contains everything except the PA–FP sshowed around 10 (6%) false positive molecules due to noise in one field of view within 3,000 camera frames (approximately 3 min). (*D*) Histogram of the number of photons emitted in each burst by mEos2 (blue) and Dendra2 (red). Photons were counted from the experiment shown in *A* and *B*. mEos2 was brighter than Dendra2 because of its longer tail. (*E*) Histogram of the number of emitted photons per molecule until photobleaching. If the molecule blinks, the number is given by the combination of multiple bursts, and thus the localization accuracy is improved when all the bursts are correctly identified as being from the same molecule.

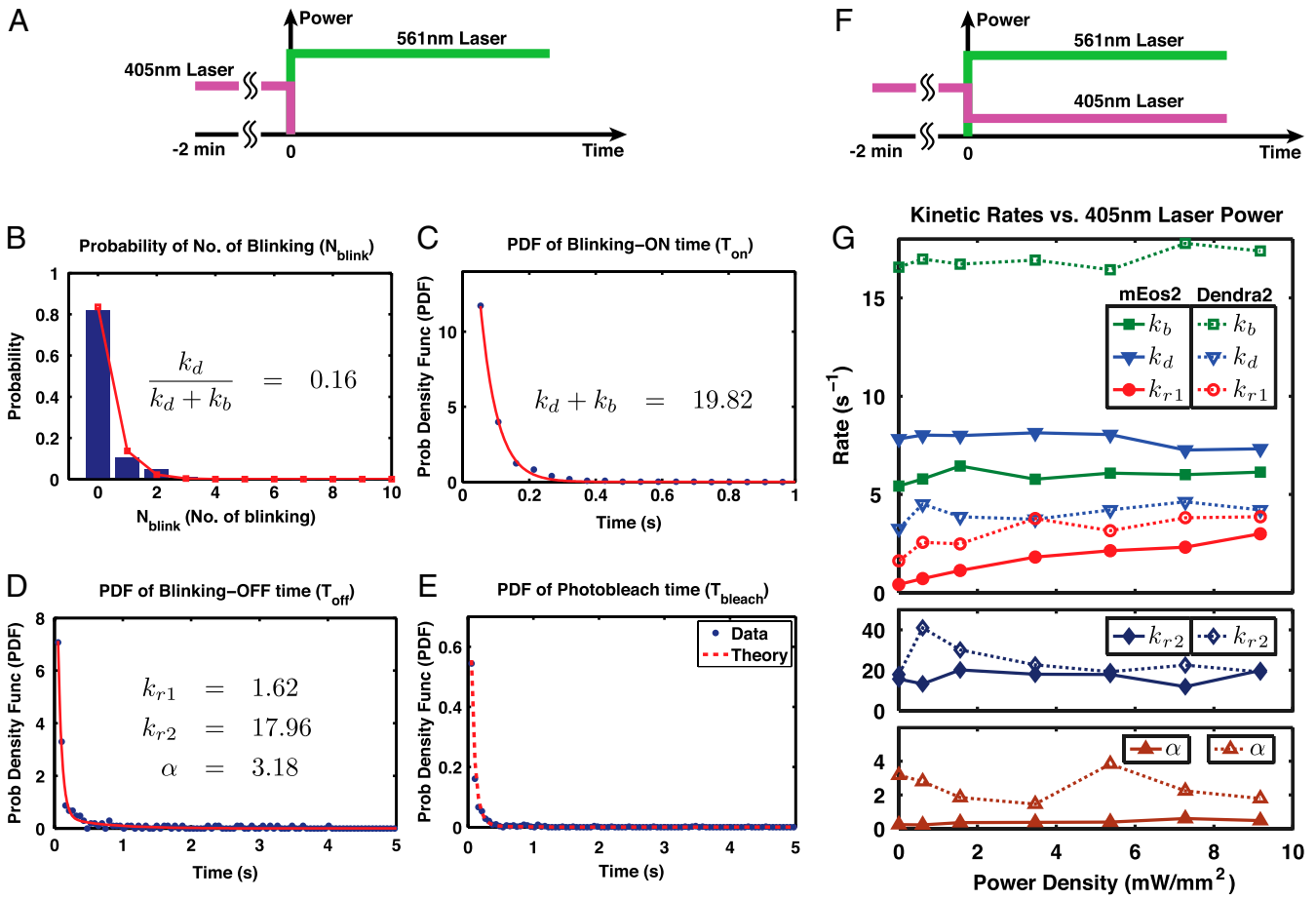

Fig. S4. (*A*–*E*) Fluorescence blinking rates of Dendra2. (*A*) Sample illumination scheme. (*B*) The histogram of the number of blinks (blue bar) fits well (red line) to the predicted geometric distribution [Eq. **S14**], where $\eta = 0.16$ is the relative probability of transition to the dark states. (*C*) The distribution of blinking-on time can be well-fitted to a single exponential. (*D*) The dwell time in the dark states (blue dots) fits well to a double exponential (red line). Actually, a single exponential function [$R^2 = 0.98$, summed square of residuals (SSE) $= 0.86$, root mean squared error (RMSE) $= 0.068$] fits the data reasonably well although a double exponential function ($R^2 = 0.99$, SSE $= 0.37$, RMSE $= 0.045$) fits it better. Therefore, the existence of two dark states is not as substantial for Dendra2 as for mEos2. We still used the double exponential fitting for Dendra2 to compare the fitted recovery rates with the values for mEos2. (*E*) Our proposed kinetic model in Fig. 2*A* and Eqs. **S24**–**S26** predict well (red dots) the distribution of photobleach time (blue dots). Here, 730 single molecules were analyzed. (*F* and *G*) Effect of 405 nm laser power on the kinetic rates of mEos2 and Dendra2. (*F*) We photoconverted all the mEos2 or Dendra2 to the activated form by intense 405 nm laser (9.1 mW/mm^2) for 2 min. Thereafter, the sample was excited with the 561 nm laser (22 W/mm^2), while the power of the 405 nm laser was set to a fixed value (0, 1.5, 3.4, 5.3, 7.2, or 9.1 mW/mm^2). (*G*) mEos2 (solid lines) and Dendra2 (dotted lines) blinking kinetic rates k_b, k_d and k_{r2}, were almost independent of the power of the 405 nm laser over that range of variation. However, the slow recovery rate of mEos2, k_{r1}, increased around 2.5 times for 9.1 mW/mm^2 of 405 nm laser power compared to when the laser was off (solid red line). This behavior is in agreement with a previous observation (1). The parameter α is also insensitive to changes in the 405 nm laser power.

1 Annibale P, Scarselli M, Kodiyan A, Radenovic A (2010) Photoactivatable fluorescent protein mEos2 displays repeated photoactivation after a long-lived dark state in the red photoconverted form. *J Phys Chem Lett* 1:1506–1510.

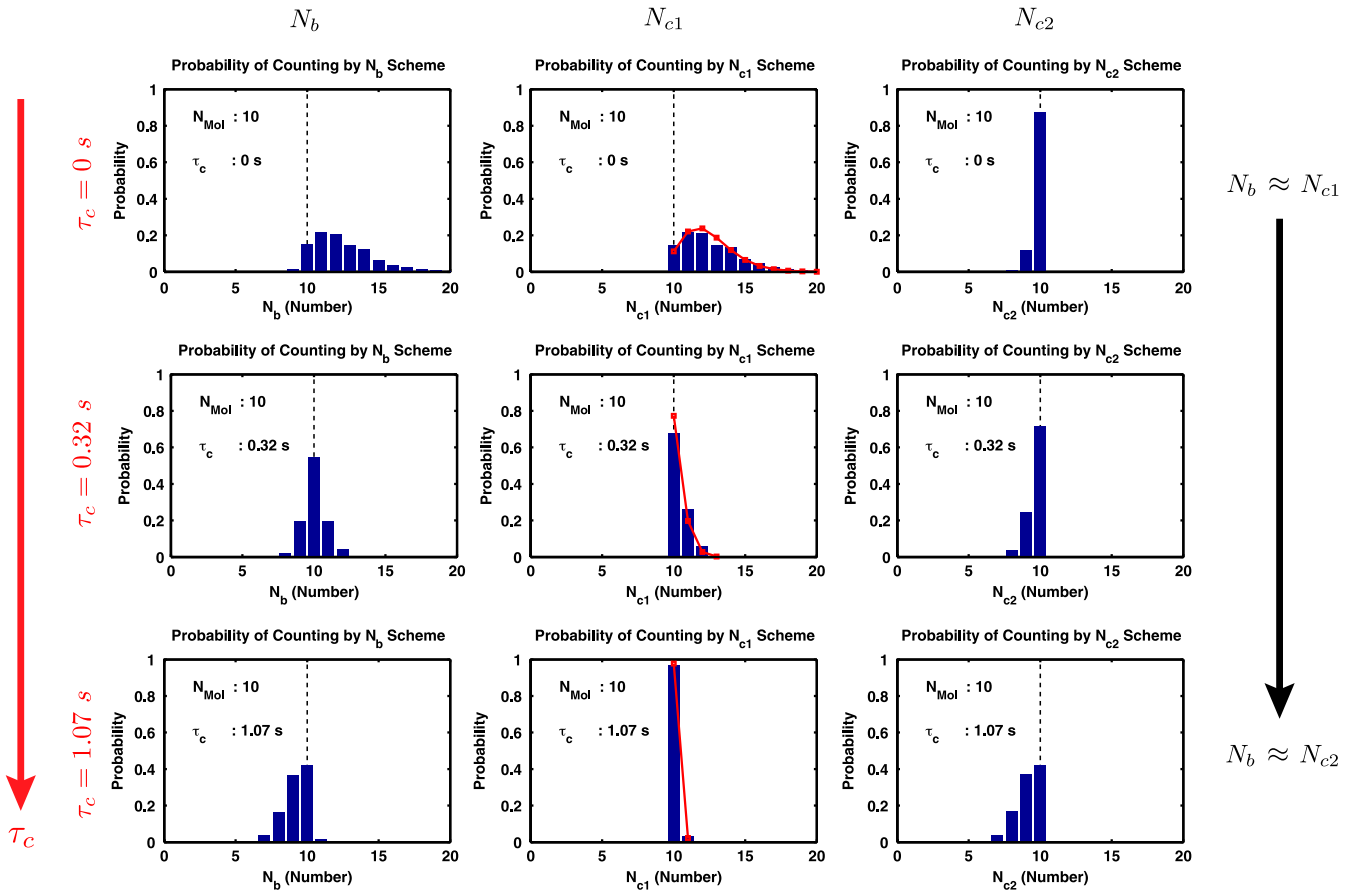

Fig. S5. Effect of τ_c on the molecular counting error for Dendra2. The counting test was carried on as described in the main text. As τ_c increases (red arrow), the distribution of N_b shifts from right to left, representing the errors dominated by overcounting (*Top Left*) and undercounting (*Bottom Left*). Therefore, the distribution of N_b values is bounded by those of N_{c1} and N_{c2}, and gets asymptotically identical to either N_{c1} or N_{c2} for extreme values of τ_c (black arrow). In particular, the value of $\tau_c = 0.32$ s makes the mean of the distribution almost match the real number of molecules, 10 (dotted line). This value of τ_c balances the error of overcounting single molecules, N_{c1}, and of undercounting by mixing different molecules, N_{c2}. A negative binomial distribution [Eq. **S41**] predicts well (red line) the probability distribution of N_{c1}. The probability distributions of N_b and N_{c2} are too complicated to be expressed analytically.

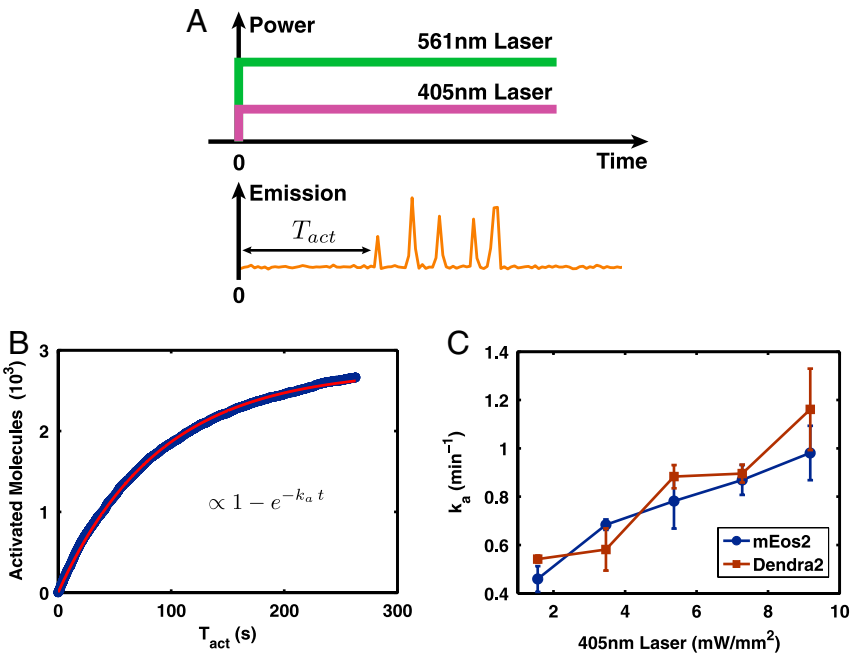

Fig. S6. Photoactivation rate measurement. (*A*) Sample illumination scheme. To study the photoactivation kinetics of PA-FPs, we used the conventional PALM illumination scheme in which both the excitation and the activation lasers are turned on at the start of data acquisition. (*B*) The temporal growth curve of the

number of activated mEos2 molecules fits well to an exponential cumulative distribution. The photoactivation rate k_a is determined from the fit. The 405 nm laser power was 3.5 mW/mm^2. (*C*) The measured photoactivation rates of mEos2 and Dendra2 are both linear with the power of the activation laser. The very similar activation rates of mEos2 and Dendra2 would be ascribed to the common peptide cleavage mechanism (1) involved in the photoactivation of the PA-FPs.

1 Nienhaus K, Nienhaus GU, Wiedenmann J, Nar H (2005) Structural basis for photo-induced protein cleavage and green-to-red conversion of fluorescent protein EosFP. *Proc Natl Acad Sci USA* 102:9156–9159.

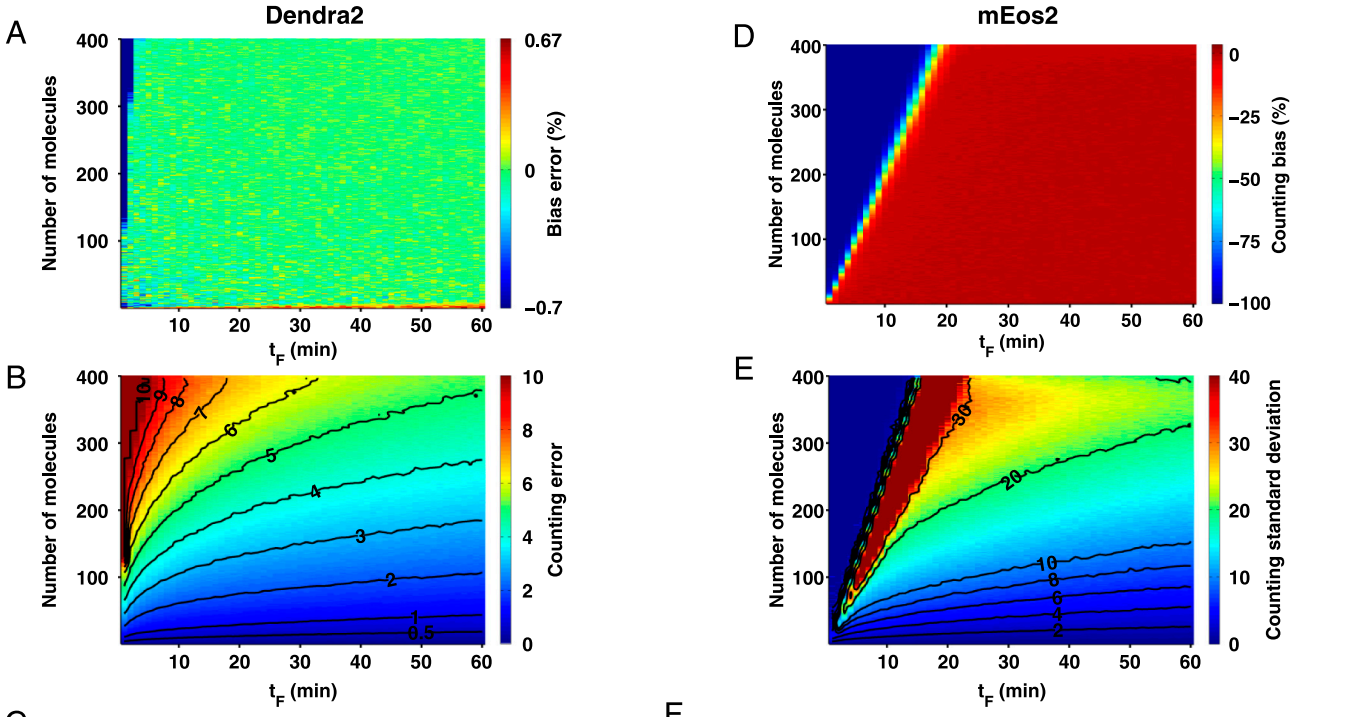

C

N_{mol} \ t_F (min)	5	10	20	30	40	50	60
5	0.36	0.28	0.22	0.20	0.18	0.17	0.17
10	0.61	0.50	0.41	0.36	0.34	0.32	0.28
20	1.06	0.91	0.74	0.65	0.59	0.55	0.50
50	2.00	1.74	1.53	1.34	1.25	1.21	1.11
100	3.38	2.85	2.49	2.24	2.12	1.99	1.92
200	5.85	4.94	4.08	3.71	3.54	3.30	3.24
300	8.02	6.91	5.52	5.09	4.47	4.41	4.18
400	9.77	8.31	7.03	6.04	5.79	5.38	5.15

F

N_{mol} \ t_F (min)	5	10	20	30	40	50	60
5	1.13	0.89	0.65	0.50	0.48	0.42	0.44
10	2.28	1.61	1.29	1.04	0.95	0.86	0.83
20	4.27	3.31	2.42	2.12	1.75	1.69	1.52
50	10.44	7.90	5.60	4.80	4.37	3.99	3.49
100	40.48	14.19	10.65	9.08	8.03	8.01	6.85
200	0.28	90.28	19.92	15.86	15.47	14.13	12.96
300	0.19	1.22	28.65	23.64	21.26	19.99	19.03
400	0.23	0.37	148.28	22.74	22.04	20.55	19.70

Fig. S7. The accuracy of the counting (color bar) depends on the number of molecules N_{mol} and the duration of the experiment t_F. We estimated the accuracy by running our iterative optimal-τ_c counting method on 1,500 simulated emission traces for each combination of N_{mol} and t_F, based on the measured kinetic parameters of Dendra2 (Fig. 2*G*). (*A*) The bias error of our counting method for Dendra2 is lower than 1.1 molecule, or 0.7% for counting up to 400 molecules if the experimental time is at least 3 min (Fig. 5). (*B*) Therefore, the main source of error is the standard deviation of the count, which is less than 10 molecules for counting up to 400 Dendra2 molecules if the experimental time is at least 5 min; it is usually much lower than that. (*C* and *F*) Tabulated values of the standard deviation (expressed in number of molecules) for a given number of molecules of (*C*) Dendra2 and (*F*) mEos2 and experimental time. Such a table enables researchers to choose the duration of their experiment based on the expected number of proteins and the desired accuracy. For example, $t_F = 10$ min is enough to count 100 Dendra2 molecules with an uncertainty of three molecules. (*D*) The bias error for mEos2 is much larger (up to 100%) than for Dendra2, (compare the left part of plots *A* and *D*), because the fluorescence traces overlap with each other even for small values of τ_c. (*E*) The standard deviation of the count, which is the other component of the counting error, is also larger for mEos2. Note that the region with low standard deviation on the left does not imply a better counting accuracy, as it is also the region where the bias is large. (All contour lines were smoothed and color maps saturated).

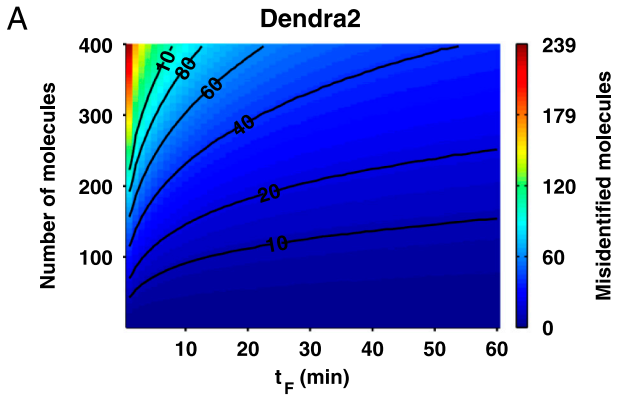

C

N_{mol} \ t_F (min)	5	10	20	30	40	50	60
5	0.20	0.18	0.10	0.08	0.09	0.07	0.06
10	0.75	0.57	0.45	0.37	0.37	0.35	0.33
20	1.60	1.29	1.05	0.81	0.72	0.64	0.56
50	5.65	4.27	3.27	2.69	2.42	2.19	1.92
100	16.20	11.38	8.69	7.29	6.38	5.85	5.39
200	45.05	32.23	22.93	19.37	17.07	15.56	14.44
300	81.14	58.70	42.13	34.71	30.28	27.74	25.68
400	121.92	89.89	64.63	52.72	45.77	41.61	38.46

D

N_{mol} \ t_F (min)	5	10	20	30	40	50	60
5	1.65	1.10	0.71	0.64	0.50	0.46	0.42
10	4.61	3.25	2.13	1.68	1.34	1.25	1.00
20	12.02	9.33	6.49	5.13	4.14	3.67	3.21
50	38.08	32.97	25.74	21.39	18.33	16.20	14.51
100	83.28	76.59	65.29	57.41	51.50	46.77	42.65
200	174.29	166.88	153.28	140.97	131.37	122.68	114.95
300	265.66	258.39	243.31	229.91	217.69	207.17	196.83
400	359.50	351.39	335.81	321.32	306.93	295.10	283.26

Fig. S8. The number of misidentified molecules depends on the actual number of molecules N_{mol} and the duration of the experiment t_F. We estimated the accuracy of identification by using our iterative optimal-τ_c counting method on 1,500 simulated emission traces for each combination of N_{mol} and t_F, based on the measured kinetic parameters of Dendra2 (Fig. 2*G*). (*A*) For Dendra2, the fraction of misidentified molecules is lower than 25% for up to 400 molecules as long as t_F is at least 10 min, and gets even lower for a smaller number of molecules; moreover, increasing the experimental time helps diminishing this error. (*B*) On the contrary, for mEos2, the fraction of misidentified molecules is much higher, and increasing the experimental time does not help much. (All contour lines were smoothed, and color maps saturated.) (*C* and *D*) Tabulated values of the number of misidentified molecules for a given molecular number of (*C*) Dendra2 or (*D*) mEos2 and a given experimental time. For example, with $t_F = 10$ min, out of 50 molecules of Dendra2, less than 10% (4.27) will be misidentified (either because some part of the emission signal is not taken into account, or because the emission signal is mixed with the one of another molecule); for mEos2, the percentage of misidentified molecules in the same configuration would be much higher (66%).

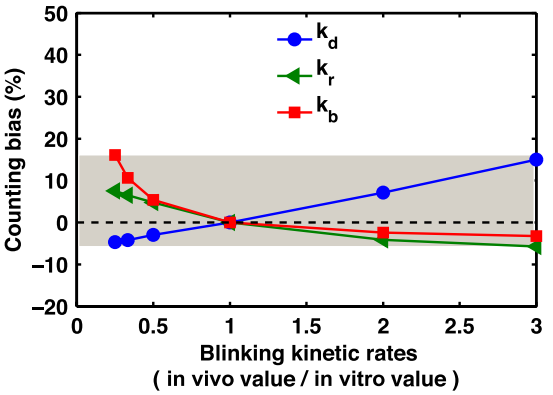

Fig. S9. Effect of the variations in the blinking kinetic rates of Dendra2 on the counting error. Multiple sets of emission traces were computer generated while varying one of the blinking kinetic rates (k_d, k_r or k_b) from its in vitro value by a factor ranging from $\frac{1}{4}$ to 3, and keeping the other rates at their in vitro values. This figure shows the percentile counting bias error incurred as a function of ratio between the assumed in vivo rate and the measured in vitro value (k_d, blue; k_r, green; k_b, red), when using the in vitro rates for the determination of the optimal-τ_c calibration curve. A change by a factor of 3 of any single kinetic rate leads to an error of less than 18% (shaded area). (We set $N_{mol} = 34$, which is the expected number of FliM molecules per flagellar motor, and $t_F = 2.2$ min, the value used in the experiments of Fig. 6).